tetracene molecules are also aligned with their molecular planes perpendicular to the FeOCl layers. Thus, one requirement for metallic conductivity in organic conductors, namely, that the donors be crystallized in segregated stacks, has been achieved for these materials. The guests molecules are very nearly close packed within the interlayer region of FeOCl.

Strong vibronic absorptions are observed in the IR spectra of $FeOCl(PE)_{1/9}$ and $FeOCl(TET)_{1/12}$. The IR data for these materials show that charge transfer from guest to host occurs during the intercalation process and that the guest species may be present as radical cations within the FeOCl galleries. This is further borne out by the observed semiconducting behavior of the intercalates. The room-temperature conductivities of $FeOCl(PE)_{1/9}$ and $FeOCl(TET)_{1/12}$ are 10^5 greater than that of FeOCl, presumably due to the electrons added to the host lattice upon oxidation of the guest species. Current work in our laboratory is focused on developing methods for controlling the degree of charge transfer in these and related materials.

Acknowledgment. This work was supported in part by the National Science Foundation, Solid State Chemistry Grant DMR-8313252. We thank Dr. K. Manus Wong for the measurement of temperature-dependent conductivity data and Dr. J.-M. Fabre, T. E. Sutto, and Dr. R. F. Bryan for helpful discussions.

Supplementary Material Available: Elemental analysis and X-ray diffraction data for the intercalates, and FTIR spectrum of $FeOCl(TET)_{1/12}$ (3 pages); F(obs) vs F(calc) for $FeOCl(PE)_{1/9}$ (1 page). Ordering information is given on any current masthead page.

X-ray Photoelectron Spectroscopy Studies of Solvated Metal Atom Dispersed Catalysts. Monometallic Iron and Bimetallic Iron-Cobalt Particles on Alumina

Beng Jit Tan, Kenneth J. Klabunde,* and Peter M. A. Sherwood*

Department of Chemistry, Willard Hall, Kansas State University, Manhattan, Kansas 66506

Received October 19, 1989

XPS studies of solvated metal atom dispersed (SMAD) catalysts coupled with detailed studies of reference compounds of iron metal, FeO, Fe_2O_3, Fe_3O_4, and FeOOH were carried out. It is shown that toluene-solvated iron atoms nucleate at surface OH groups of the Al_2O_3 catalyst support. The resultant iron oxide surface species served as nucleation sites for deposition of more iron atoms, leading to very small metallic iron clusters/particles. A thin oxide layer was detected on the particle surface that is believed to come from adventitious oxygen. When toluene-solvated cobalt and iron atoms were allowed to mix and nucleate together, iron reacted with and deposited on surface OH groups first. Then nucleation of Co and Fe occurred together on these surface iron oxide sites, with a slight excess of iron on the inside part of the particle. The iron oxide served as a gradient between the ionic support oxide and metallic iron/cobalt. Mössbauer spectroscopy confirmed the metallic nature of SMAD iron particles (unsupported).

Introduction

By using solutions of solvated metal atoms of limited thermal stability, we have been able to prepare very highly dispersed heterogeneous catalysts of Fe,[1] Co-Mn,[2,3] Ni,[4] Pt-Sn,[5] Pt-Re,[6] and other metallic particles on various catalyst supports.[7-9,11] Bimetallic systems have proven particularly interesting, exhibiting remarkable catalytic activities where one metal can have a significant effect on the other. Those unusual properties stem from unique particle structures (e.g., cobalt layers on manganese),[8] high dispersion,[9] and the ability of one metal to behave sacrificially for the other.[8]

In this study we deal with iron-solvated metal atom dispersed (SMAD) catalysts and iron-cobalt combinations. This combination was chosen for their similar oxophilicity and stabilities as solvated atoms in toluene. We wished to learn if such similar metals would yield alloy-like particles by the SMAD method or whether layered structures would result, with one metal acting sacrificially (being oxidized by support OH groups) to preserve the other in a nonoxidized, metallic state.[10]

Experimental Section

Materials. Metals were obtained from Matheson, Coleman, and Bell (iron) and Cerac, Inc. (cobalt) in high purity forms. The support used was American Cyanamid γ-Al_2O_3 (200 m^2/g) and was calcined at 773 K for 3 h in flowing dry air (420 mL/min) and cooled in flowing nitrogen (500 mL/min). Purified deoxygenated toluene was used exclusively as the codeposition solvent for the metal atoms. Commerically available (Alfa Products) metals, metal oxides, and hydroxides were used as reference compounds.

Catalyst Preparation. The metal vapor reactor and catalyst preparation methods have been described earlier.[4,5,9,12] Metal loadings on Al_2O_3 are given in the text and tables.

XPS Experiments. Sample preparation and handling have been described earlier.[8a] Our XPS measurements were made using an AEI ES200B spectrometer with a base pressure of better than

(1) Kanai, H.; Tan, B. J.; Klabunde, K. J. *Langmuir* **1986**, *2*, 760.
(2) Klabunde, K. J.; Imizu, Y. *J. Am. Chem. Soc.* **1984**, *106*, 2721.
(3) Imizu, Y.; Klabunde, K. J. In *Catalysis of Organic Reactions*; Augustine, R. L., Ed.; Marcel Dekker: New York, 1985.
(4) Matsuo, K.; Klabunde, K. J. *J. Catal.* **1982**, *73*, 216.
(5) Li, Y. X.; Klabunde, K. J. *Langmuir*, **1987**, *3*, 558.
(6) Ahkmedov, V.; Klabunde, K. J. *J. Mol. Catal.* **1988**, *45*, 193.
(7) Klabunde, K. J.; Tanaka, Y. *J. Mol. Catal.* **1983**, *21*, 57, and references therein.
(8) (a) Tan, B. J.; Klabunde, K. J.; Tanaka, T.; Kanai, H.; Yoshida, S. *J. Am. Chem. Soc.* **1988**, *110*, 5951. (b) Tan, B. J.; Klabunde, K. J.; Sherwood, P. M. A. *J. Am. Chem. Soc.*, submitted. (c) McIntrye, N. S.; Cook, M. G. *Anal. Chem.* **1975**, *47*, 1975.
(9) Matsuo, K.; Klabunde, K. J. *J. Org. Chem.* **1982**, *47*, 843.
(10) Woo et al. (Woo, S. J.; Godber, J.; Ozin, G. A. *J. Mol. Catal.* **1989**, *52*, 241 have very recently reported on the interaction of solvated iron atoms with silica O-H surface groups.
(11) Li, Y. X.; Zhang, Y. F.; Klabunde, K. J. *Langmuir* **1988**, *4*, 385.
(12) Klabunde, K. J.; Timms, P. L.; Skell; P. S.; Ittel, S. *Inorg. Synth.* **1979**, *19*, 59. Shriver, D. (editor) gives a general description of metal atom vapor chemistry.

0897-4756/90/2802-0186$02.50/0

Table I. XPS Binding Energies (eV)[a,b] for Iron Reference Compounds

sample	Fe($2p_{3/2}$)	Fe($2p_{1/2}$)	O(1s)
Fe_2O_3	710.7 (4.7)	723.9 (4.3)	529.6 (1.5)
Fe_3O_4	710.1 (4.8)	723.4 (3.8)	529.5 (1.5)
FeOOH	711.4 (4.7)	724.2 (4.2)	531.5 (1.4), 529.5 (1.4)
FeO[c]	709.3	722.8	520.6
Fe metal	706.8 (1.1)	720.1 (1.3)	

[a] Values in parentheses are full width at half-maximum (fwhm). [b] Error limits are ±0.2 eV. [c] Average value obtained from literature, after correcting to C(1s) 284.6 eV.

10^{-9} Torr using Mg Kα X-radiation. Spectra were recorded to achieve maximum instrument resolution (better than 0.8 eV), and data were usually collected with at least 17 points per electrovolt in order to be sure to identify any subtle features than might be lost at lower resolution and a larger step size. Binding energies were calibrated by using C 1s from residual carbon in the samples taken as 284.6 eV. Spectra were fitted by using a nonlinear least-squares program with a 50% mixed Gaussian–Lorentzian product function.[13] XPS intensity ratios were determined by using total integrated areas of the Fe(2p), Co(2p), O(1s), and Al(2p) photoelectron lines. Peak area computation was performed after a nonlinear background was removed.[14] Difference spectra were obtained and normalization was performed by using our previously described method.[14] The peak area ratios were calculated taking into account the Scofield photoelectron cross sections.[15]

Results

Iron Reference Compounds. XPS has the potential to distinguish between metallic iron, various iron oxides, and iron hydroxides. The oxides and hydroxides differ in crystallographic structures and oxygen to iron ratio and also in the relative concentration of Fe^{2+} and Fe^{3+} and their distribution between octahedral and tetrahedral lattice sites.

Table I summarizes the binding energies of reference oxides, hydroxides, and metallic iron determined in this study. Our values agree with previously reported values.[31]

Much literature on the XPS characterization of iron and its oxides is available, and the area has been fully reviewed by Wandelt,[31] including the characterization of commercially available iron oxide powders,[16-19] iron oxides formed by thermal decomposition of iron oxalate,[20,21] oxide films formed on metal substrates,[22-24] single-crystal studies,[25,26] surface treatment of iron oxide powders with Ar^+ ion etching,[27,28] attempts to separate the oxidation states in Fe_3O_4,[28,29] studies of α- and γ-Fe_2O_3.[30] Agreement among the literature values for the binding energy data for iron and its oxides is good.

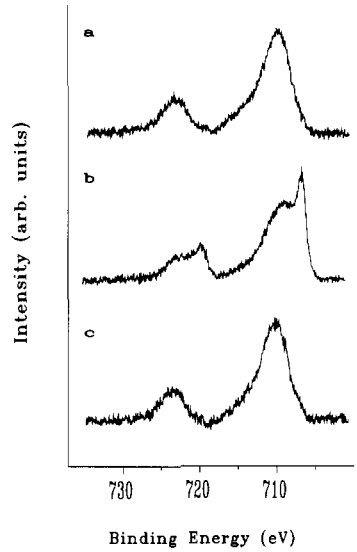

Figure 1. Fe(2p) XPS spectra of SMAD unsupported Fe catalyst: (a) fresh sample; (b) argon ion etched for 2 min; and (c) after exposing the argon-etched sample to air for 5 min.

Previous studies show Fe 2p core level chemical shift values for the oxides FeO and Fe_3O_4 are sufficiently large to permit them to be distinguished from Fe_2O_3 (with Fe($2p_{3/2}$) for Fe(III) being 710.8 eV and for Fe(II) being 709.3 eV), but it is not possible to clearly distinguish FeOOH from Fe_2O_3.

We find[32] that FeOOH and Fe_2O_3 can be distinguished from their valence band spectra and by differences in the O(1s) and O(2s) regions.

The Fe(2p) peaks of the reference compounds show steep background and non-Gaussian peak shapes and were found to be rather broad due to satellite features and multiplet splitting.[31] This is also true of the SMAD catalysts as we shall see later. The average half widths obtained were 4.8 and 4.4 eV (±0.2 eV) for the Fe($2p_{3/2}$) and Fe($2p_{1/2}$) peaks, respectively.

Unsupported SMAD Iron Catalyst Particles. Figure 1 shows the background-subtracted XPS spectra of the fresh unsupported SMAD Fe catalyst (Figure 1a), after a 2-min Ar^+ ion etch (Figure 1b), and after exposing the etched sample to air for 5 min (Figure 1c). Table II summarizes the electron binding energies of Fe(2p), O(1s), and C(1s) regions of the unsupported SMAD Fe catalyst as it goes through these different stages.

The Fe 2p region for the fresh catalyst sample suggested that the surface corresponded to Fe_3O_4 with a small shoulder on the lower binding energy side corresponding to metallic iron. After a 2-min Ar^+ ion etch, the Fe($2p_{1/2}$)/Fe($2p_{3/2}$) region showed two peaks at 706.8 and 709.1 eV, which correspond to the presence of metallic iron and FeO/Fe_3O_4, respectively. Exposing the etched sample to air at ambient conditions oxidized the metallic iron to its oxides, and the main peak moved to the higher binding energy (Figure 1c). The binding energy of the fe(2p) peak was now even higher than that of the original sample, probably indicating formation of more surface Fe_2O_3 on exposure to air. However, a shoulder at lower binding energy corresponding to metallic iron indicated that complete oxidation of the catalyst had not taken place.

The assignment of metallic iron in Figure 1b is supported by difference spectra (see Figure 2, which shows the difference to correspsond to iron). We thus conclude

(13) Sherwood, P. M. A. In *Practical Surface Analysis by Auger and X-ray Photoelectron Spectroscopy*; Briggs, D., Seah, M. P.; Eds., Wiley: New York, 1983; Appendix 3.
(14) (a) Proctor, A.; Sherwood, P. M. A. *Anal. Chem.* **1980**, *52*, 2315. (b) Proctor, A.; Sherwood, P. M. A. *Anal. Chem.* **1982**, *54*, 13.
(15) Scofield, J. H. *J. Electron. Spectrosc. Relat. Phenom.* **1976**, *8*, 129.
(16) Allen, G. C.; Curtis, M. T.; Hooper, A. J.; Tucker, P. M. *J. Chem. Soc., Dalton Trans.* **1974**, 1525.
(17) Yabe, K.; Arata, K.; Toyoshima, I. *J. Catal.* **1979**, *57*, 231.
(18) Hirokawa, K.; Oku, M. *Talanta* **1979**, *26*, 855.
(19) Vasudevan, S.; Hegde, M. S.; Rao, C. N. R. *J. Solid State Chem.* **1979**, *29*, 253.
(20) Asami, K.; Hashimoto, K.; Shimodaira, S. *Corros. Sci.* **1976**, *16*, 35.
(21) Asami, K.; Hashimoto, K. *Corros. Sci.* **1977**, *17*, 559.
(22) Allen, G. C.; Tucker, P. M.; Wild, R. K. *Philos. Mag.* **1982**, *46*, 411.
(23) Ertl, G.; Wandelt, K. *Surf. Sci.* **1975**, *50*, 479.
(24) Brundle, C. R. *Surf. Sci.* **1977**, *66*, 581.
(25) Brundle, C. R.; Chuang, T. J.; Wandelt, K. *Surf. Sci.* **1977**, *68*, 459.
(26) Oku, M.; Hirokawa, K. *J. Appl. Phys.* **1979**, *50*, 5303.
(27) Kurtz, R. L.; Henrich, V. E. *Surf. Sci.* **1983**, *129*, 345.
(28) McIntyre, N. S.; Zetaruk, D. G. *J. Vac. Sci. Techol.* **1977**, *14*, 181.
(29) McIntyre, N. S.; Zetaruk, D. G. *Anal. Chem.* **1977**, *49*, 1521.
(30) Oku, M.; Hirokawa, K. *J. Electron. Spectrosc. Relat. Phenom.* **1976**, *8*, 475.
(31) Wandelt, K. *Surf. Sci. Rep.* **1982**, *2*, 69–77.
(32) Welsh, I. D.; Sherwood, P. M. A. *Phys. Rev. B* **1989**, *40*, 6386.

Table II. XPS Binding Energies (eV)[a] for Unsupported Fe SMAD Catalyst

treatment	Fe($2p_{3/2}$)		Fe($2p_{1/2}$)		O(1s)			C(1s)	
fresh	706.8	709.1	720.1	723.5	532.6 (2.0)	531.2 (2.0)	529.6 (1.5)	288.2 (1.7)	284.6 (1.7)
etched	706.8	709.1	720.1	722.8		531.3 (1.7)	529.6 (1.7)	288.4	286.3
								284.6 (1.7)	283.3 (1.7)
air exposed	706.8	710.3	720.1	723.7	532.8 (1.9)	531.3 (1.9)	529.5 (1.6)	288.2 (1.7)	284.6 (1.7)

[a] Values in parentheses are fwhm.

Table III. XPS Binding Energies (eV)[a] for SMAD Fe/Al_2O_3 Catalysts

catalyst	Fe($2p_{3/2}$)	Fe($2p_{1/2}$)	C(1s)		Al(2p)
2.0% Fe	710.3	723.0	531.6 (3.1)	529.6 (3.1)	74.5 (2.5)
3.2% Fe	710.1	723.0	531.4 (3.0)	529.5 (3.0)	74.5 (2.4)
4.7% Fe	709.9	723.0	531.3 (2.8)	529.5 (2.8)	74.5 (2.5)
5.8% Fe	710.1	723.1	531.5 (3.0)	529.6 (3.0)	74.5 (2.4)

[a] Values in parentheses are fwhm.

that the unsupported SMAD Fe catalyst consisted of an inner metallic core and surface oxide species.

The O(1s) envelope consisted of three components at 529.6, 531.2, and 532.6 eV attributable, respectively, to iron oxides, hydroxide species from absorbed water, and adsorbed oxygen.[31] After argon ion etching, the Fe(2p)/O(1s) area ratio doubled and the relative intensity of the peak attributed to adsorbed water decreased with respect to the oxide peak while the peak corresponding to adsorbed oxygen disappeared.

The C 1s spectrum of the fresh catalyst showed some adsorbed CO.

SMAD Iron Catalysts Supported on Alumina. Some examples of Fe(2p) spectra of SMAD Fe/Al_2O_3 catalysts are shown in Figure 3. A nonlinear background has been removed. The figure shows three sets of spectra, fresh catalysts in the left column, the etched (2-min argon ion) catalysts in the center, and the difference spectra in the right column. The difference spectra were obtained by subtracting a normalized spectrum of the fresh catalysts from that of the etched catalyst. A shoulder was seen on the high binding energy side of the Fe($2p_{3/2}$) peak for catalysts with low metal loadings. This shoulder decreased in intensity as the metal loading was increased. This shoulder is attributed to the shakeup satellite in Fe_2O_3, about 8 eV higher in binding energy than the Fe($2p_{3/2}$) peak. There is also a small shift of the Fe 2p peak to lower binding energy as the metal loading increased due to the formation of larger amounts of lower oxidation state oxides. Table III lists the binding energies of the Fe(2p), Al(2p), and O(1s) peaks in some of the fresh samples analyzed.

Argon ion etching the SMAD Fe/Al_2O_3 catalysts removed surface hydrocarbon, revealing more of the underlying catalyst surface. The spectrum consisted of several components at 706.8 and about 710.0 eV attributed to metallic iron and a mixture of FeO and Fe_3O_4, respectively. Table IV lists the binding energies of the Fe(2p), O(1s), and Al(2p) regions of the etched samples.

The intensity of the metallic iron peak in these etched catalysts samples increases with metal loading. It can be easily seen that as the metal loading increases, the statistics of the difference spectrum is improved and the amount of metallic iron increases (Figure 3).

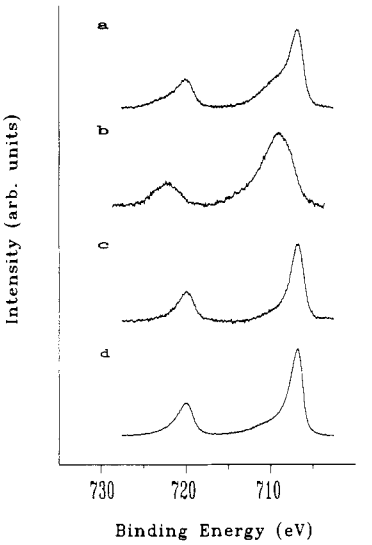

Figure 2. Spectral subtraction on the unsupported SMAD catalyst: (a) argon-ion-etched sample; (b) fresh sample; (c) result of spectral subtraction (a–b) (normalization factor = 0.82); (d) iron foil.

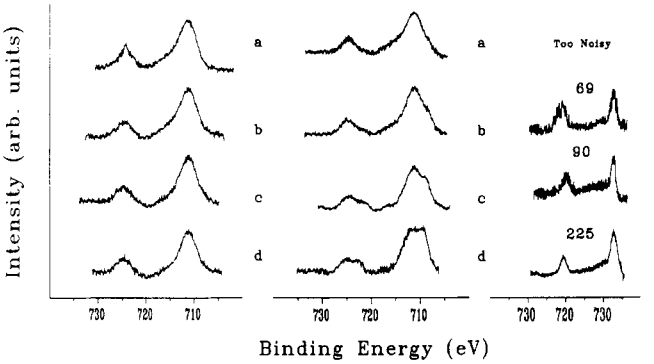

Figure 3. Fe(2p) XPS spectra for SMAD Fe/Al_2O_3 catalysts with a nonlinear background removed: (a) 2.0% Fe; (b) 3.2% Fe; (c) 4.7% Fe; (d) 5.8% Fe. The spectra in the left column are those of the fresh catalysts, while the spectra of the argon ion etched catalysts are shown in the middle column. The difference spectra, obtained by the subtraction of the spectra of the fresh catalysts from their corresponding etched catalysts are shown in the right column. The normalized areas of the difference spectra are indicated.

As listed in Table V the Fe($2p_{3/2}$)/Al(2p) intensity ratio increased with iron loading.

SMAD Iron–Cobalt Catalysts Supported on Alumina. A similar experimental treatment and analysis was

Table IV. XPS Binding Energies (eV)[a] for SMAD Fe/Al_2O_3 Catalysts after a 2-min Argon-Ion Etch

catalyst	Fe($2p_{3/2}$)		Fe($2p_{1/2}$)		C(1s)		Al(2p)
2.0% Fe	706.8	710.0	720.1	723.1	531.6 (2.9)	529.7 (2.9)	74.5 (2.4)
3.2% Fe	706.8	710.0	720.1	723.1	531.5 (3.0)	529.5 (3.0)	74.5 (2.5)
4.7% Fe	706.8	709.5	720.1	723.1	531.6 (2.6)	529.7 (2.6)	74.5 (2.5)
5.8% Fe	706.8	709.3	720.1	722.8	531.6 (3.0)	529.7 (3.0)	74.5 (2.5)

[a] Values in parentheses are fwhm.

Table V. XPS Fe(2p)/Al(2p) Peak Area Intensity Ratios for SMAD Fe/Al_2O_3 Catalysts

	fresh		etched	
catalyst	Fe(2p)/O(1s)	Fe(2p)/Al(2p)	Fe(2p)/O(1s)	Fe(2p)/Al(2p)
2.0% Fe	0.27	0.56	0.42	0.59
3.2% Fe	0.26	0.72	0.38	0.82
4.7% Fe	0.24	0.83	0.32	0.89
5.8% Fe	0.31	0.93	0.45	0.98

applied to the SMAD Fe–Co/Al_2O_3 catalysts. The Fe(2p) spectra (Figure 4) of the fresh and argon ion etched (2-min etch) bimetallic Fe–Co/Al_2O_3 catalysts resemble those of the monometallic Fe/Al_2O_3 catalysts. Tables VI and VII summarize the binding energies of the fresh and etched Fe–Co/Al_2O_3 catalysts, respectively.

The surface species on these bimetallic SMAD Fe–Co catalysts was found to be a mixture of Fe_2O_3 and Fe_3O_4. Also, as the percentage of Fe loading increased, the shoulder characteristic of Fe_2O_3 decreased in intensity. Again, a 2 min Ar^+ ion etch resulted in exposing metallic iron and a shift of the Fe(2p) peak corresponding to the mixture of oxides toward lower binding energy.

The iron composition of the Fe–Co/Al_2O_3 catalysts is similar to the monometallic Fe/Al_2O_3 catalysts, namely, an inner metallic core surrounded by a layer of surface oxides. Results from spectral subtraction of the fresh catalyst's spectra from the corresponding etched catalyst samples showed that the intensity of the subtracted spectrum increases with metal loading and that the difference spectrum resembles the metallic iron XPS spectrum. One important difference between the monometallic and bimetallic catalysts of equal iron metal loading is a higher amount of metallic iron in the bimetallic catalysts (compare normalized metal intensities on Figures 3 and 4). Also, we can conclude that the presence of cobalt does not seem to have any effect on the nature of surface iron species of the bimetallic Fe–Co catalysts.

As Table VIII shows, the Fe($2p_{3/2}$) intensity ratio of the fresh catalyst samples increased with metal loading, just as was observed with the monometallic systems.

The Co(2p) spectra of the fresh sample, the etched catalysts, and the difference spectra (obtained by subtracting a weighted fraction of the spectrum of the fresh catalyst from its corresponding argon ion etched sample) are shown in Figure 5, and data are summarized in Tables IX and X. The Co surface species was cobalt hydroxide as evident from the Co(2p) and O(1s) XPS regions and the characteristic $Co(OH)_2$ spectral feature.[8c]

An increase in the Co/Fe content ratio (Table XI) was accompanied by an increase in the normalized Co(2p) peak area intensity of the difference spectrum (Figure 5).

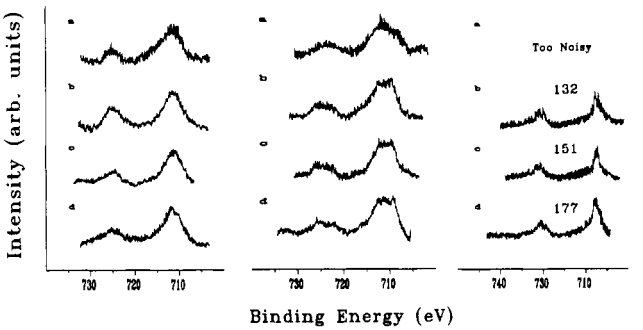

Figure 4. Fe(2p) XPS spectra of Co–Fe/Al_2O_3 catalysts: (a) 3.9% Co–4.3% Fe; (b) 4.0% Co–3.3% Fe on SiO_2; (c) 3.9% Co–2.6% Fe; (d) 4.0% Co–1.6% Fe. The spectra in the left column are those of the fresh catalysts, while the spectra of the argon-ion-etched catalysts are shown in the middle column (a and d etched 2 min, b 90 s, c 3 min). The difference spectra, obtained by the subtraction of the spectra of the fresh catalysts from their corresponding etched catalysts are shown in the right column. The normalized areas of the difference spectra are indicated.

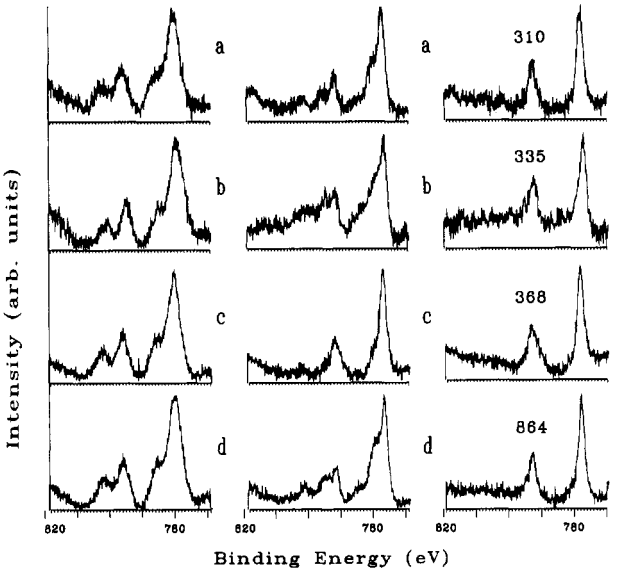

Figure 5. Co(2p) XPS spectra of Co–Fe/Al_2O_3 catalysts: (a) 3.9% Co–4.3% Fe; (b) 4.0% Co–3.3% Fe on SiO_2; 3.9% Co–2.6% Fe; (d) 4.0% Co–1.6% Fe. The spectra in the left column are those of the fresh catalysts while the spectra of the argon-ion-etched catalysts are shown in the middle column (a and d etched 2 min, b 90 s, c 3 min). The difference spectra, obtained by the subtraction of the spectra of the fresh catalysts from their corresponding etched catalysts, are shown in the right column. The normalized areas of the differnece spectra are indicated.

Slightly shorter etch time (b, 90 s) give relatively less Co metal compared to the 2-min etch time (a, d), and longer

Table VI. XPS Binding Energies (eV)[a] for SMAD Fe–Co/Al_2O_3 Catalysts

catalyst	Fe($2p_{3/2}$)	Fe($2p_{1/2}$)	O(1s)		Al(2p)
4.0% Co–1.6% Fe	710.3	723.6	531.5 (3.0)	529.6 (3.0)	74.5 (2.5)
3.9% Co–2.6% Fe	710.1	723.5	531.5 (2.8)	529.6 (2.8)	74.5 (2.5)
4.0% Co–3.3% Fe[b]	710.0	723.2	531.6 (2.5)	529.5 (2.5)	74.5 (2.4)
3.9% Co–4.4% Fe	710.4	723.4	531.5 (2.9)	529.6 (2.9)	74.5 (2.4)

[a] Values in parentheses are fwhm. [b] On SiO_2.

Table VII. XPS Binding Energies (eV)[a] for SMAD Fe–Co/Al_2O_3 Catalysts after a 2-min Argon Etch

catalyst	Fe($2p_{3/2}$)		Fe($2p_{1/2}$)		O(1s)		Al(2p)
4.0% Co–1.6% Fe	706.8	708.3	720.1	722.6	531.4 (2.9)	529.6 (2.9)	74.5 (2.4)
3.9% Co–2.6% Fe	706.8	709.3	720.1	722.8	531.7 (2.8)	529.7 (2.8)	74.5 (2.6)
4.0% Co–3.3% Fe[b]	706.8	709.6	720.1	723.1	531.6 (2.4)	529.7 (2.4)	74.5 (2.5)
3.9% Co–4.4% Fe	706.8	709.8	720.1	723.2	531.7 (2.9)	529.6 (2.9)	74.5 (2.5)

[a] Values in parentheses are fwhm. [b] On SiO_2.

Table VIII. XPS Peak Area Ratios for SMAD Fe–Co/Al_2O_3 Catalysts

	fresh		etched	
catalyst	Fe(2p)/Al(2p)	Fe(2p)/Co(2p)	Fe(2p)/Al(2p)	Fe(2p)/Co(2p)
4.0% Co–1.6% Fe	0.17	0.13	0.19	0.14
3.9% Co–2.6% Fe	0.38	0.23	0.42	0.36
4.0% Co–3.3% Fe[a]	0.45	0.45	0.48	0.38
3.9% Co–4.4% Fe	0.72	0.36	0.69	0.45

[a] On SiO_2

etch time (3 min) gives more Co metal (c).

Discussion

Our earlier work[8a,b] with SMAD Co–Mn catalysts showed that the more oxophilic metal, manganese, deposited on the support first, scavenging oxidizing moieties and protecting cobalt from a similar fate. So our work with Fe and Co mixtures was prompted by two things: (1) to find out if iron, only slightly more oxophilic than cobalt, would be able to serve the same function that manganese did; (2) to try to gain understanding of changes in catalytic properties of Fe–Co/support over Fe/support or Co/support systems.[2,3]

Since metal oxide formation plays an important role in catalyst particle structure (and presumably affecting catalytic activity as well), we need to ascertain why oxides form. There are, of course, two possible ways: (1) adventitious oxygen that is encountered during catalyst isolation and preparation for XPS analysis. Our samples are prepared in a hydrocarbon (toluene) medium, which is a reducing environment, and the toluene-solvated metal atoms (1 and 2) nucleate on the support surface. Excess

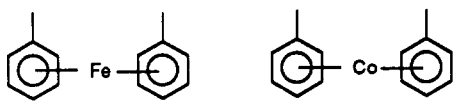

1 2

toluene is removed under vacuum, and the resultant dry powders were handled in an oxygen-free environment throughout the entire process of preparing samples and placing in the XPS instrument. However, these SMAD samples are extremely oxophilic and even trace amounts of oxygen could be scavenged, and such trace amounts lead to the apparently very thin layers of oxides, hydroxides, H_2O, and O_2 on the surfaces of the particles. (2) Another, actually advantageous, source of oxidation are surface OH groups on the catalyst support. On higher surface area Al_2O_3 pretreated at 500 °C, enough OH groups are present to completely oxidize a 3–4% loading of cobalt (or manganese).[8a,b] Thus, we can rationalize why low loadings of Fe/Al_2O_3 show mainly oxides (eq 1).

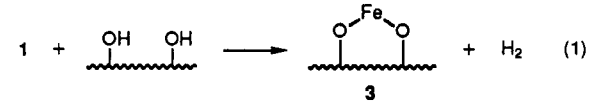

With these ideas in mind we will now examine the XPS data reported here.

The unsupported Fe SMAD particles showed the presence of metallic iron and FeO after a 2-min argon ion etch. Such a short etch period should only remove about a ~ 10–20-Å layer of surface impurities, mainly adventitious carbonaceous material often found on surfaces examined by XPS.[33] On the basis of literature sources[29,30] and on our own experiments on reference iron compounds, we

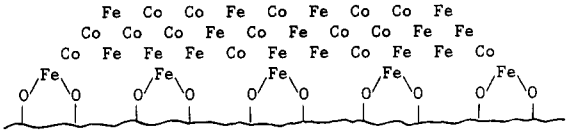

Figure 6. Model for a SMAD Fe–Co/Al_2O_3 particle ignoring surface oxides.

conclude that a very thin FeO/Fe_3O_4 layer covers a large metallic core for these particles. Indeed, Mössbauer spectroscopy supports this model. This bulk sample analysis technique showed the characteristic six-line spectrum for metallic α-Fe.[34] Thus, when no support (and no surface OH groups) was present, rather large metallic iron particles formed that became covered with a thin oxide layer, perhaps 10–20 Å thick. These are the expected results and were verified by experiment.

Turning now to Fe/Al_2O_3 systems, we note that the conventional iron salt impregnation method followed by the necessary hydrogen reduction processes yielded a material that showed only surface Fe_2O_3 by XPS analysis.[35] In our SMAD Fe/Al_2O_3 system the surface species present depends on percent metal loading. The decrease in the shakeup satellite in Fe_2O_3 as iron content increased shows that lower oxidation state oxides became predominant (our results and literature[31] have shown that Fe_3O_4 shows no satellite structure). Argon ion etching (only 2 min) allowed metallic iron to be observed, and the intensity of this peak increased dramatically on going from 3.2% to 5.8% Fe (Figure 3). Likewise, an increase in the Fe(2p)/Al(2p) peak intensity ratio was observed with increase in metal loading, suggesting a more uniform and more concentrated layer of iron on the Al_2O_3 surface. That is, as iron loading increases, additional nucleation sites are employed *and* metallic particles sizes are enhanced.

For the bimetallic Fe–Co/Al_2O_3 catalysts, an increase in the Fe(2p)/Al(2p) ratio with increase in Fe loading can be attributed to an increase in iron dispersion on the surface, as found for the monometallic system discussed above.

Interestingly, the Fe(2p)/Co(2p) peak ratio generally increased for the SMAD Co–Fe/support catalysts upon etching (Table VIII). Also, from Table XI we note that the Co(2p)/Fe(2p) ratio is very high, initially ranging from 2.2 to 7.7. These data indicate that the surface of the metal particles is richer in cobalt than in iron and that underneath the surface more iron is present. This means that during formation of the SMAD catalysts, the first portion of solvated iron atoms nucleates first (before cobalt) on the Al_2O_3 surface. After the surface has been pacified by iron deposition (now in an oxidized state), the remaining solvated iron and cobalt atoms nucleate together on the iron-bearing surface sites[36] (eq 2). The final particle

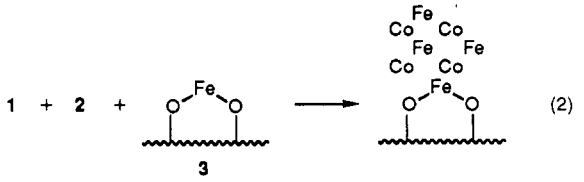

structure is similar to that found for Mn–Co systems, ex-

(33) Breeze, P. A.; Hartnagel, H. L.; Sherwood, P. M. A. *J. Electrochem. Chem. Soc.* **1980**, *127*, 454.

(34) Tan, B. J. Ph.D. Thesis, Kansas State University, 1989. Further bulk analyses techniques, such as Mössbauer and EXAFS, will be reported later with H. Kanai, T. Tanaka, and S. Yoshida.

(35) Lacquaniti, V.; Battistoni, C.; Paparazzo, E.; Cocito, M.; Palumbo, S. *Thin Solid Films* **1982**, *94*, 331.

(36) The findings of Woo et al.[10] are supported by ours; that is, iron atoms/clusters are oxidized by surface OH groups.

Table IX. XPS Parameters (eV)[a] for SMAD Co-Fe/Al_2O_3 Catalysts

catalyst	peak 1 MP	peak 1 SS	peak 1 ΔS	peak 2 MP	peak 2 SS	peak 2 ΔS	Δ	Al(2p)
4.0% Co-1.6% Fe	780.8	786.2	5.4	796.4	802.1	5.7	15.5	74.5 (2.5)
3.9% Co-2.6% Fe	780.8	786.3	5.5	796.3	802.1	5.8	15.5	74.5 (2.5)
4.0% Co-3.3% Fe[b]	781.0	786.6	5.6	796.3	802.2	5.9	15.3	74.3 (2.4)
3.9% Co-4.4% Fe	780.9	786.4	5.5	796.4	802.1	5.7	15.5	74.6 (2.4)

[a] Values in parentheses are fwhm. MP, binding energy of the main peak; SS, binding energy of the satellite peak; ΔS, energy separation of the satellite from the main peak; Δ, spin-orbit splitting. [b] On SiO_2.

Table X. XPS Parameters (eV) for SMAD Co-Fe/Al_2O_3 Catalysts after Argon-Ion Etching[a]

catalyst	Co($2p_{3/2}$) MP		Co($2p_{3/2}$) SS	Co($2p_{3/2}$) ΔS	Co($2p_{1/2}$) MP		Co($2p_{1/2}$) SS	Co($2p_{1/2}$) ΔS	Δ	
4.0% Co-1.6% Fe	777.9	781.0	786.2	5.2	792.7	796.5	802.1	5.6	14.8	15.5
3.9% Co-2.6% Fe	777.9	780.9	786.3	5.4	792.7	796.4	802.0	5.6	14.7	15.5
4.0% Co-3.3% Fe[b]	777.9	780.8	786.3	5.5	792.6	796.6	802.1	5.5	14.7	15.8
3.9% Co-4.4% Fe	777.9	780.9	786.2	5.3	792.7	796.5	802.1	5.6	14.8	15.6

[a] MP, binding energy of main peak; SS, binding energy of satellite peak; ΔS, energy separation between the satellite peak and the main peak; Δ, spin-orbit splitting. [b] On SiO_2.

Table XI. XPS Peak Area Intensity Ratios for SMAD Co-Fe/Al_2O_3 Catalysts

catalyst	fresh Co(2p)/Al(2p)	fresh Co(2p)/Fe(2p)	etched Co(2p)/Al(2p)	etched Co(2p)/Fe(2p)
4.0% Co-1.6% Fe	0.16	7.7	0.13	7.1
3.9% Co-2.6% Fe	0.16	4.3	0.12	2.8
4.0% Co-3.3% Fe[a]	0.12	2.2	0.16	2.6
3.9% Co-4.4% Fe	0.16	2.8	0.13	2.2

[a] On SiO_2.

cept with a less pronounced layering and Fe and Co intimately mixed in the metallic portion of the particles (Figure 6). It should be pointed out, though, that iron enrichment at the support surface is real but only partial, since the presence of cobalt did allow more metallic iron to persist in the catalysts. Thus, iron sacrifices itself mostly for preservation of metallic cobalt, but cobalt does the same thing for iron to a smaller extent. Figure 6 illustrates an idealized Fe–Co/Al_2O_3 SMAD particle, ignoring the thin layer of metal oxides on the metal particle surface.[37]

Conclusions

(1) Iron SMAD catalysts with very low loadings are almost completely oxidized by the support surface OH groups. In this way, iron is anchored to the catalyst surface.

(2) With Fe–Co combinations, a partial layering was observed where mainly iron deposits on the support surface whereupon Co and Fe nucleate on the ironized sites. In the metallic phase Fe and Co are mixed, but on progressing deeper into the catalyst particle iron richness increases. In this way, as we observed for Co–Mn systems,[8a,b] the more oxophilic metal concentrates at the ionic oxide (support) surface so that the layering tends toward inorganic oxide support, then oxide (FeO and Fe_3O_4), from the less oxophilic metal, and then metallic iron and cobalt. This is another example of a "graded seal" type of catalyst and may help explain the very good stability of SMAD catalysts toward sintering.

(3) These results show that toluene solvated iron and cobalt atoms do not deposit according to their thermal stability (1 about −30 °C and 2 about −50 °C). Since iron preferentially deposits first, the reaction of 1 with support surface OH groups must be the dominant driving force for deposition and thereby nucleation of particle growth.

(4) These preferential layering tendencies are not as strong with Fe and Co as they are with Mn and Co. Iron is more sacrificial than cobalt, however.

Acknowledgment. The generous support of the National Science Foundation is gratefully acknowledged. We also acknowledge helpful discussions with Hiroyoshi Kanai of Kyoto University.

Registry No. Fe, 7439-89-6; Co, 7440-48-4.

(37) Although we have not been successful in using TEM to measure particle sizes directly, chemisorption and EXAFS studies of other, similar bimetallic particles (e.g., Co–Mn) have consistently given particle sizes of 10–25 Å, with the smaller sizes probably favored.